Periodicity in the autocorrelation function as a mechanism for regularly occurring zero crossings or extreme values of a Gaussian process

Lorna R. M. Wilson[*]

Institute for Mathematical Innovation, University of Bath, Bath, England, United Kingdom

Keith I. Hopcraft

Department of Mathematical Sciences, University of Nottingham, Nottingham, England, United Kingdom

The problem of zero crossings is of great historical prevalence and promises extensive application. The challenge is to establish precisely how the autocorrelation function or power spectrum of a one-dimensional continuous random process determines the density function of the intervals between the zero crossings of that process. This paper investigates the case where periodicities are incorporated into the autocorrelation function of a smooth process. Numerical simulations, and statistics about the number of crossings in a fixed interval, reveal that in this case the zero crossings segue between a random and deterministic point process depending on the relative time scales of the periodic and nonperiodic components of the autocorrelation function. By considering the Laplace transform of the density function, we show that incorporating correlation between successive intervals is essential to obtaining accurate results for the interval variance. The same method enables prediction of the density function tail in some regions, and we suggest approaches for extending this to cover all regions. In an ever-more complex world, the potential applications for this scale of regularity in a random process are far reaching and powerful.

I. INTRODUCTION

One-dimensional, continuous random processes are used to model a huge variety of real world phenomena. In particular, the zero crossings of such processes are relevant to problems such as diffusion [1], signal processing [2], speech analysis [3], fault detection [4], radio waves [5], ocean waves [6,7], hydrology [8], meteorology [9], genetics [10], and finance [11,12]. Zero crossings have also impacted on queuing theory [13], reliability theory [14], and applied probability [15,16].

Not only do zero crossings provide information about return times and threshold crossings, but they also tell us about extreme values. This is because the turning points of one random process occur at the same time as the zeros of the derivative of that process.

Blake and Lindsey [17] commented, in a review of the zero-crossing problem, that "the ultimate goal of such an investigation would be to determine the probability density of the lengths of the intervals between zeros of the process" and noted that "very little success has been achieved in finding this function." Over 40 years on, this is still very much the case. The only analytical result for the density of interval times is particular to a Gaussian process with a specific autocorrelation function [18].

In this paper we consider smooth, Gaussian processes which are fully characterized by the autocorrelation function and straightforward to simulate. We make the autocorrelation function our starting point for investigation, choosing a particular oscillatory form introduced previously in conference proceedings [19], and motivated in the next section. Statistics for the number of zero crossings occurring within a set time period are calculated and verified by simulations of the process. These demonstrate that such periodicities in the autocorrelation function describe a process for which the zero crossings segue between a random and deterministic point process—this is a result with great potential for application. We extend the work of McFadden [20,21] to describe the interval variance and density function in this particular case. We present our results and explore the limitations of these methods.

The interplay between randomness and order is a pervasive component of the dialogue surrounding complex systems; it is present in the type of exploratory behavior observed by ants [22], or the development of the circulatory and nervous systems [23,24]. The precise way in which components interact both randomly and deterministically determines the emergent behavior of the system as a whole. This balancing act between random exploration and deterministic exploitation has been hypothesized to be a general property of intelligent, adaptive systems [25]. Furthermore, continuous one-dimensional random processes are often an effective way to build randomness, whatever its origin, into a model. Their most established application is in signal processing, and much of the mathematical theory was developed with this in mind. Real-world continuous processes frequently prove difficult to measure and analyze in full, and it can be informative to observe only their crossings, reducing them to a series of points in time, or a point process. By linking a continuous Gaussian process to a random point process, the regularity of which is directly determined by the autocorrelation function, the work of this paper presents a valuable modeling tool.

II. PERIODICITY AND THE AUTOCORRELATION FUNCTION

The autocorrelation function (or the corresponding power spectrum) describes the memory of the process and is essential

_____

[*]L.Wilson@bath.ac.uk

to the determination of the statistical properties of the process and its zero crossings. For a stationary process $X(\tau)$ with zero mean, the autocorrelation function is independent of the origin of time and given by

$$\rho(\tau') = \frac{\langle X(0)X(\tau')\rangle}{\sigma^2}$$

where σ^2 is the variance of the process. It is a real valued function satisfying $|\rho(\tau')| \leqslant \rho(0)\ \forall \tau'$ with $\rho(0) = 1$ and as $\tau' \to \infty$, $\rho(\tau') \to 0$. Due to the stationarity of the process $X(\tau)$, $\rho(\tau')$ is symmetric about the origin. Finally, the power spectrum of the correlation model, which describes how the variance of $X(t)$ is distributed over its frequency components, must be positive definite. The power spectrum $\bar{\rho}(\omega)$ is given by the Wiener-Khinchin theorem [26–28] as the Fourier transform of $\rho(\tau)$:

$$\bar{\rho}(\omega) = 2 \int_0^\infty \rho(t) \cos(2\pi\omega t) dt. \tag{1}$$

When prescribing an autocorrelation function it must satisfy all of these properties and so the power spectrum may place constraints on the allowable values of any parameters of $\rho(\tau)$.

For the mean rate of zero crossings to exist, the autocorrelation function must be twice differentiable at the origin, i.e., $\rho(\tau) = 1 - b\tau^2 + O(\tau^{2+\mu})$ with $b, \mu > 0$. If this is not the case then the autocorrelation describes a fractal process, where an infinite number of zero crossings fails to be resolved by magnification [29]. Where this is the case, and $0 < \mu < 2$, the resulting process is known as subfractal. This is because the mean rate of zero crossings of the process itself exists, but the mean rate does not exist for the differentiated process which exhibits fractal behavior. In the case where $\mu = 2$, the process is smooth and all derivatives exist. It is these smooth processes with which this paper is concerned.

In order to motivate the precise form of autocorrelation we have chosen to investigate, we first consider the signal $S(t)$ formed by a Gaussian process $G(t)$, modulated by a cosinusoidal wave with a random phase shift. The signal exhibits interplay between the random behavior of $G(t)$ and deterministic, periodic behavior governed by the cosine. Zeros resulting from the random process break up the regular crossings of the cosine.

We define the signal $S(t)$:

$$S(t) := \sqrt{2}\cos(at + \phi_0)G(t) \tag{2}$$

where $\phi_0 \sim U(0, 2\pi)$ is a uniformly distributed random phase fixed in time, and $G(t)$ is an independent, stationary Gaussian process with zero mean, unit variance, and autocorrelation function $g(\tau) = \langle G(0)G(\tau)\rangle$. A realization of $S(t)$ and $G(t)$ is shown in Fig. 1.

The autocorrelation function of the signal $S(t)$ is

$$\rho_s(\tau) = \frac{\langle S(0)S(\tau)\rangle}{\sigma_s^2}$$
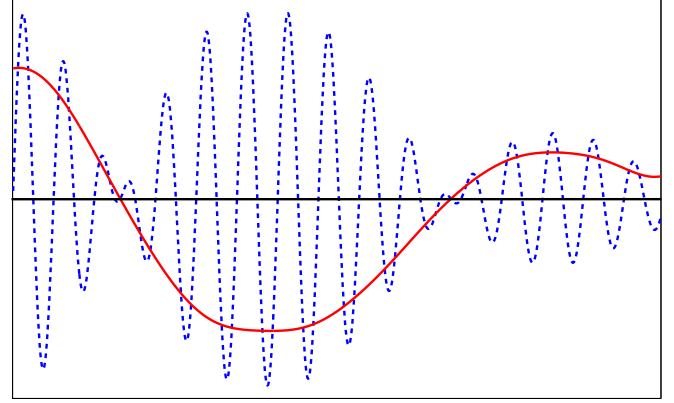$$= \frac{2\langle\cos(\phi_0)G(0)\cos(a\tau + \phi_0)G(\tau)\rangle}{\sigma_s^2}.$$

FIG. 1. A representation of $G(t)$ (solid red line) and $S(t)$ (dotted blue line).

Due to the independence of $G(t)$ and the cosine, the variance of $S(t)$ is 1. Therefore

$$\rho_s(\tau) = 2\langle\cos(\phi_0)G(0)\cos(a\tau + \phi_0)G(\tau)\rangle$$
$$= 2\langle\cos(\phi_0)\cos(a\tau + \phi_0)\rangle\langle G(0)G(\tau)\rangle$$
$$= \cos(a\tau)g(\tau).$$

The autocorrelation function $g(\tau)$ determines the behavior of the random process $G(t)$. For a smooth, twice-differentiable process a suitable choice of autocorrelation function is

$$g(\tau) = \left(1 + \frac{\tau^2}{\gamma}\right)^{-\gamma/2}$$

where γ determines the rate of decay of the memory of the process.

In this paper we consider the Gaussian process $X(t)$ with zero mean, unit variance, and the same autocorrelation function as $S(t)$:

$$\rho(\tau) = \cos(a\tau)\left(1 + \frac{\tau^2}{\gamma}\right)^{-\gamma/2}. \tag{3}$$

The process will only be considered for $\gamma \geqslant 2$ where numerical analysis reveals that the power spectrum is positive definite for all values of a.

It should be noted that, while it has the same mean and variance as $X(t)$, the signal $S(t)$ is not a Gaussian process. The probability density function (PDF) of S is

$$p(S) = \frac{1}{2\pi^{3/2}}K_0\left(\frac{S^2}{8}\right)\exp\left(-\frac{S^2}{8}\right)$$

where K_0 is a modified Bessel function of the second kind [30]. This expression for the PDF of S has a logarithmic singularity at the origin, meaning $S(t)$ spends more time near the origin than the Gaussian process $X(t)$, which by definition has a Gaussian PDF.

To summarize, $G(t)$ is a Gaussian process with zero mean, unit variance, and autocorrelation $g(\tau)$. $S(t)$ is the non-Gaussian random process obtained by modulating $G(t)$ with a cosine; it also has zero mean and unit variance. $X(t)$ is a Gaussian process with zero mean, unit variance, and the same oscillatory autocorrelation function as $S(t)$.

A. Time scales

The autocorrelation function (3) has two time scales: $\ell_1 = 1/a$ from the cosine and ℓ_2 from the power law. The power law governs the overall decay of the autocorrelation function. The "width" of this power law reflects the overall memory of the corresponding Gaussian process; it is this that the time scale ℓ_2 should capture. In the limit $\gamma \to \infty$, the power law is a Gaussian function:

$$\lim_{\gamma \to \infty} \left(1 + \frac{\tau^2}{\gamma}\right)^{-\gamma/2} = \exp\left(-\frac{\tau^2}{2}\right),$$

for which the obvious choice for the time scale is $\ell_2 = \sqrt{2}$.

The width of the power law is compared to that of the Gaussian function as follows: With argument $\tau = \sqrt{2}$, the Gaussian function is e^{-1} and this is set to be equivalent to the power law with argument ℓ_2:

$$\left(1 + \frac{(\ell_2)^2}{\gamma}\right)^{-\gamma/2} = e^{-1}.$$

It then follows that

$$\ell_2 = (\gamma e^{2/\gamma} - \gamma)^{\frac{1}{2}}. \tag{4}$$

This has the properties that $\ell_2 \to \sqrt{2}$ as $\gamma \to \infty$ and $\ell_2 \to \infty$ as $\gamma \to 0$.

It should be noted that there are alternative ways to characterize the width of the (symmetric) power-law function, for example taking a scalar multiplier of the (positive) square root of the variance of the power law. The scalar multiplier can be set so that the property $\ell_2 \to \sqrt{2}$ as $\gamma \to \infty$ is preserved, however $\ell_2 \to \infty$ as $\gamma \to 3$. Another alternative is the mean value of the power law over the positive real line. Again, the scalar multiplier can be chosen to preserve the property $\ell_2 \to \sqrt{2}$ as $\gamma \to \infty$. In this case $\ell_2 \to \infty$ as $\gamma \to 2$. All these possible time scales for the power-law function are monotonically decreasing, converge to $\sqrt{2}$ as $\gamma \to \infty$, and diverge for small values of γ. For the purposes of this paper, this is sufficient information about ℓ_2 to aid explanation of the trends observed in the corresponding Gaussian process. Further analysis of this function will require careful justification of time scales used. The formulation given by (4) is chosen here because it exists for all positive, real values of γ.

B. Mean crossing rate

A zero crossing is a sign change of a process from positive to negative values or vice versa. The mean zero-crossing rate is the expected number of zero crossings per unit time. For the Gaussian process $X(t)$, the mean rate of crossings $\bar{r}$ depends only on the second derivative of the autocorrelation function at the origin. It is calculated via the well known result first presented in Sec. 3.3 of Rice's report on "Mathematical Analysis of Random Noise" [31]:

$$\bar{r} = \frac{[-\rho''(0)]^{1/2}}{\pi} = \frac{(1+a^2)^{1/2}}{\pi}. \tag{5}$$

Note that the mean rate of crossings is independent of γ. As the autocorrelation function gets more oscillatory with increasing a, the rate of zero crossings increases.
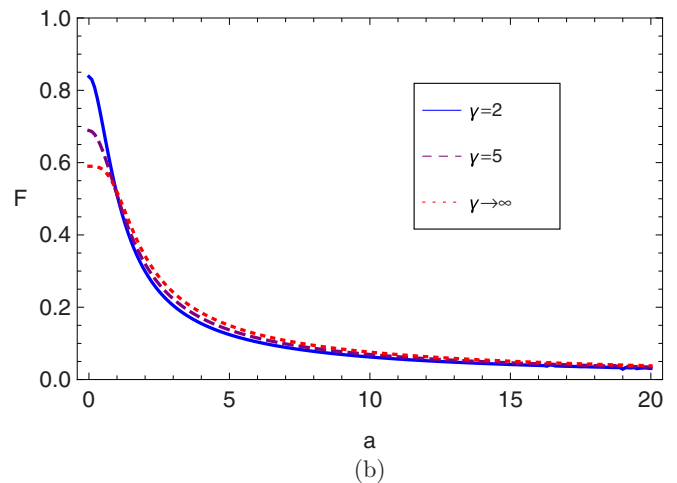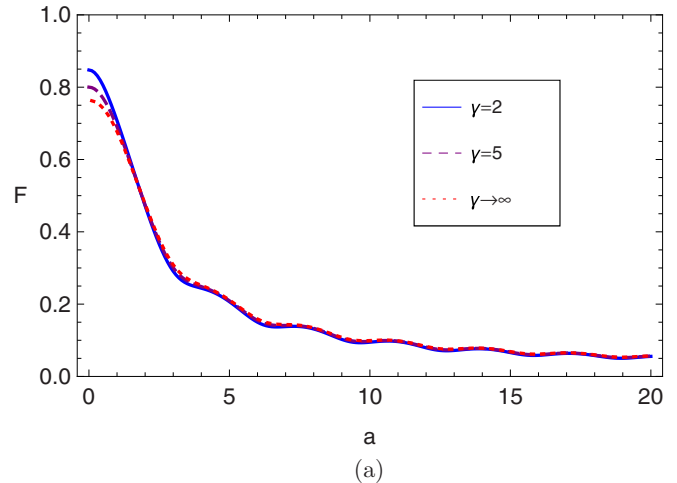

FIG. 2. Fano factor as a function of a with $\gamma = 2$, $\gamma = 5$, and $\gamma \to \infty$. (a) $T = 1$. (b) $T = 10$.

The mean rate of crossings for the signal $S(t)$ is

$$\bar{r}_s = \frac{a}{\pi} + \bar{r}_g = \frac{1+a}{\pi}.$$

In the limits $a \to 0$ and ∞, the mean rate of zero crossings of the signal $S(t)$ and the Gaussian process $X(t)$ are the same.

C. Fano factor

The fluctuations in the number N of zero crossings of a stationary process, in an interval of fixed length T, are described by the Fano factor [32]:

$$F(T) := \frac{\text{var}(N)}{\langle N \rangle} = 1 + \frac{\langle N(N-1) \rangle}{\langle N \rangle} - \langle N \rangle.$$

The Fano factor is the discrete analog of the coefficient of variation: It quantifies the departure of the fluctuations in random events occurring in a window of length T from purely Poisson statistics. It was first used in particle detection to detect deviations in dispersion of the number of ions produced by constant amounts of radiation energy. It has proved useful for characterizing neural spiking [33] and is extensively used in photonics [34]. When there are Poisson number
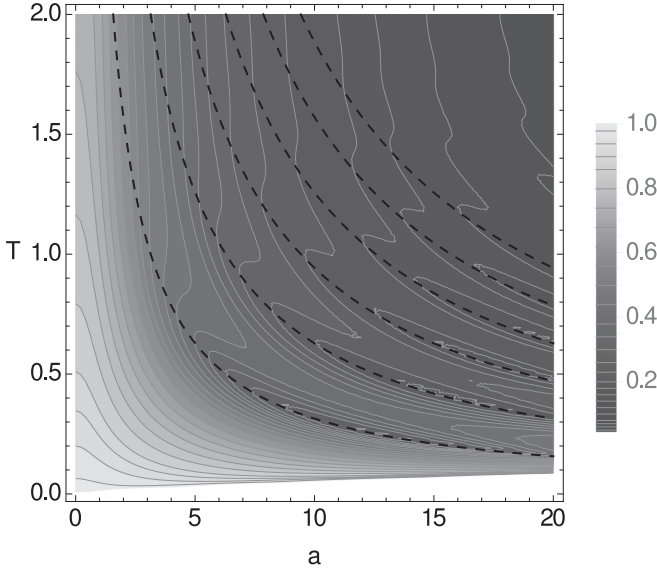
FIG. 3. F parametrized against a, and the integration time T. The dashed lines show $T = n\langle\tau\rangle$ for $n = 1$–6.

FIG. 4. F for $a = 15$ and $\gamma \to \infty$, plotted against $T\bar{r}$ so that the integer-valued grid lines correspond to $T = n\langle\tau\rangle$ for $n = 1$–8.

fluctuations, $\text{var}(N) = \langle N \rangle$ and $F(T) = 1$. If fluctuations are super-Poissonian then zeros occur in clusters and $F > 1$. In the case of sub-Poissonian behavior where zeros are repelled from each other, $F < 1$.

The Fano factor is calculated via Rice's result for the mean number of crossings (5) and the following result by Steinberg *et al.* [35]:

$$\langle N(N-1) \rangle = \frac{2T^2}{\pi^2} \int_0^1 \frac{dy(1-y)}{[1 - \rho^2(yT)]^{3/2}}$$

$$\times \left[|A^2 - B^2|^{1/2} + B \arctan\left(\frac{B}{|A^2 - B^2|^{1/2}} \right) \right]$$

where $A = -\rho''(0)[1 - \rho^2(yT)] - \rho'^2(yT)$

and $B = \rho''(yT)[1 - \rho^2(yT)] + \rho(yT)\rho'^2(yT)$. (6)

The cases $\gamma = 2$, $\gamma = 5$, and $\gamma \to \infty$ are compared in Fig. 2 for $T = 1$ and 10. The overriding trend is that, as a increases, the Fano factor decreases. For large a (i.e., when $\ell_1 \ll \ell_2$) the cosine in the autocorrelation function oscillates much faster than the power law decays. The result is that the effect of the cosine dominates the behavior of the process; there is little fluctuation in the number of zero crossings in an interval, i.e., zeros occur at more regular intervals and the process appears increasingly "deterministic."

This is reflective of the interplay between the random behavior of $G(t)$ and deterministic, periodic behavior governed by the cosine in signal $S(t)$. For small enough a, when the power law dominates the autocorrelation function, F increases with decreasing γ. When a is large enough that the oscillations in the autocorrelation function significantly affect the process, this effect is reversed and F decreases with decreasing γ. The greater the difference $\ell_1 \ll \ell_2$, the more the cosine affects the process and the more regular the zero crossings are.

For smaller values of T there are ripples in $F(a)$. This rich behavior of the Fano factor is displayed in Fig. 3. In order to understand how these ripples in the Fano factor relate to
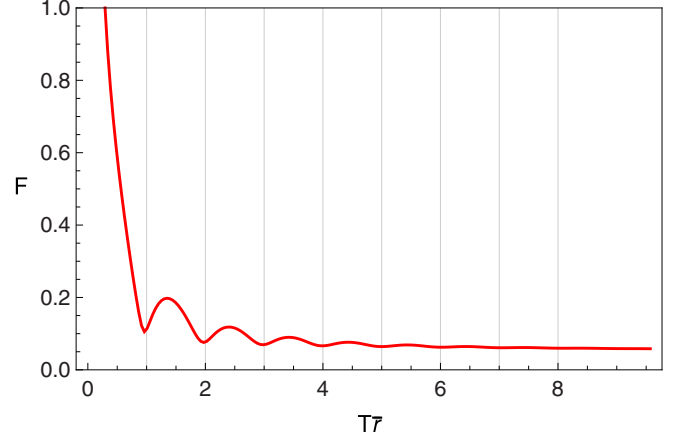
the behavior of $X(t)$ itself, we consider F as a function of T as in Fig. 4, which reveals that the first local minimum of F occurs when the fixed interval length T is equal to the mean interval between zero crossings, i.e., $T = 1/\bar{r}$. Subsequent local minima occur at $T = n/\bar{r}$ (where n takes integer values) until, with sufficiently large T, the ripples are damped. Zero crossings occur regularly for large enough a and so when $T = n/\bar{r}$ there is very little fluctuation in the number of zeros which is highly likely to be n, but when $T = (n + 1)/2\bar{r}$ there are equally likely to be n or $n + 1$ zeros in an interval. This change in fluctuation in the number of zeros means that F is locally larger when $T = (n + 1)/2$ and smaller when $T = n/\bar{r}$. This is plainly visibly in Fig. 4 where the grid lines at n correspond to the minima in F.

III. SIMULATION RESULTS

Simulations are obtained by Fourier transforming both Gaussian random noise and the autocorrelation function, then multiplying them in the frequency domain and Fourier inverting the result back into "real" space (this is equivalent to forming a convolution of Gaussian random noise and the autocorrelation function). This is an established method covered in many texts [28].

A. Variance of the intervals

Figure 5 shows simulations of the variance of the interval between successive zero crossings, for $\gamma \to \infty, \gamma = 5$, and $\gamma = 2$ in the autocorrelation function:

$$\rho(\tau) = \cos(a\tau)\left(1 + \frac{\tau^2}{\gamma} \right)^{-\gamma/2}.$$

The variance declines rapidly with increasing a, and becomes less than the mean at $a \sim 1.2$, indicating the distribution for the intervals is narrowing. The effect of γ, or equivalently the size of the power-law time scale ℓ_2, is minimal. A larger ℓ_2 will result in the power law dominating the behavior of the process until a larger cosine time scale $\ell_1 = 1/a$ (equivalent to a smaller value of a) is attained. In the region where the power law dominates the behavior of the process, a larger ℓ_2 results
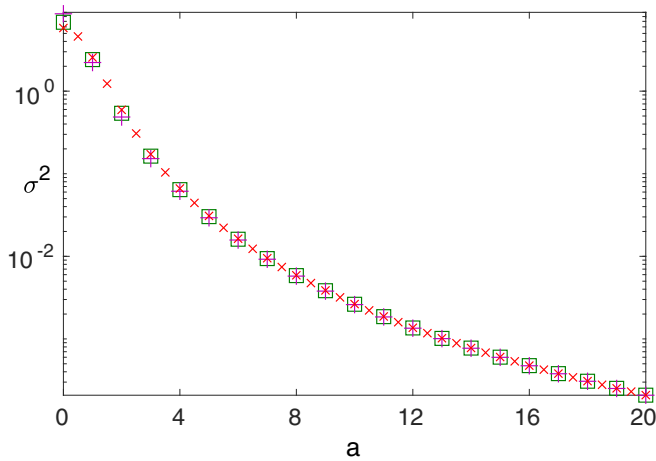
FIG. 5. Simulation results for the variance of the intervals for $\gamma \to \infty$ (purple +), $\gamma = 5$ (green □), and $\gamma = 2$ (red ×).

in a higher variance. In the region where the cosine dominates the process, the zero crossings occur more regularly and the variance is small, and the effect of ℓ_2 is negligible.

The remainder of this paper will focus on the Gaussian limit case where $\gamma \to \infty$ (or $\ell_2 \to 0$) such that

$$\rho(\tau) = \cos(a\tau) \exp\left(-\frac{\tau^2}{2}\right)$$

and $\ell_2 = \sqrt{2}$. Here, a relatively small cosine time scale ℓ_1 results in the Gaussian function dominating the behavior so that intervals have a greater variance. For ℓ_1 small enough the process will behave as if the non-oscillatory Gaussian autocorrelation function has been used. This could represent physical processes such as the scattering of light from a random-phase-changing screen [36]. A large cosine time scale ℓ_1 means the cosine dominates the behavior of the process, resulting in low interval variance and regular zero crossings. This could be representative of processes that exhibit some periodicity, such as the nearly periodic 11-year solar sunspot cycle [37].

B. Density function of the intervals

The time between zero-crossing events is a *continuous* random variable τ with $P_n(\tau)d\tau$ denoting the probability that the $(n+1)$th event occurring after time t_0 falls within the interval $t_0 + \tau$ to $t_0 + \tau + d\tau$ and $P_0(\tau)$ is the density of the interval length between successive events. Figure 6 shows three plots of simulations of the interevent density function $P_0(\tau)$. Figure 6(a) shows $P_0(\tau)$ for values of a from zero to twenty. As a increases, the mean decreases and the PDF shifts to smaller values of τ in accordance with (5). In addition, the PDF becomes more concentrated around the mean, reflecting the greater regularity of the zero crossings. This is better observed in Fig. 6(b), which shows the renormalized PDF plotted on the rescaled axis $\tau/\langle\tau\rangle$. The previous sections showed that, with increasing a, successive intervals become highly correlated i.e., $\kappa \to 1$ and $\sigma^2 \to 0$ as $a \to \infty$. These simulation results confirm that the corresponding effect on the PDF is that $P_0(\tau)$ tends towards a delta function located at the mean interval spacing $\tau = \langle\tau\rangle$.
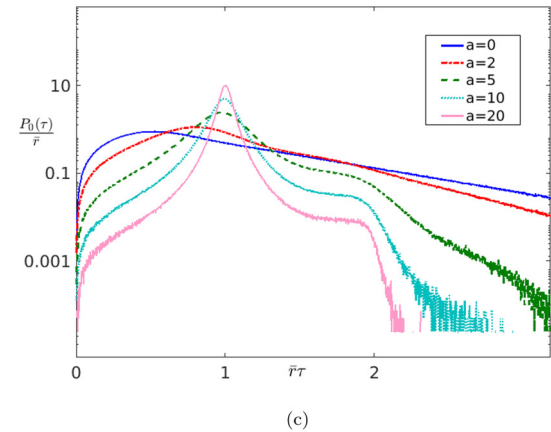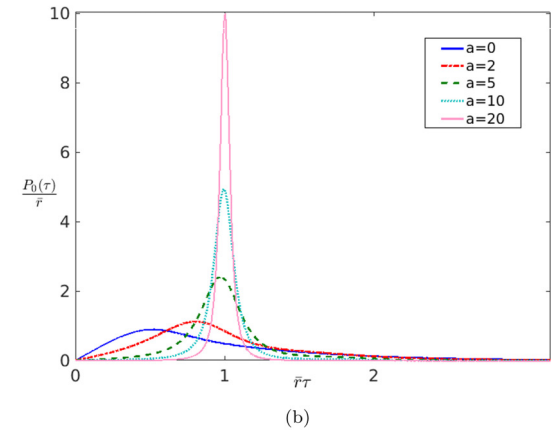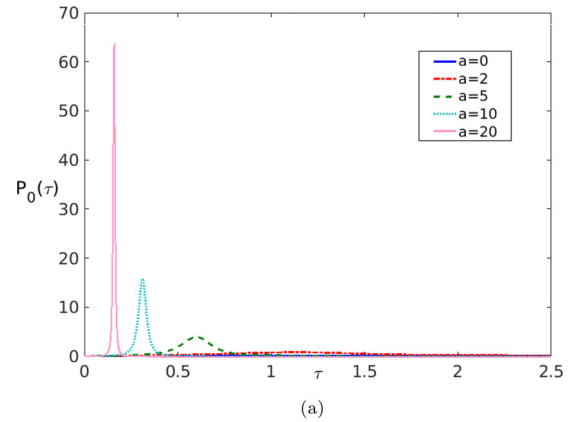

(a)

(b)

(c)

FIG. 6. Simulations of the interval density function $P_0(\tau)$ for $a = 0, 2, 5, 10$, and 20. (a) $P_0(\tau)$. (b) Renormalized simulations of $P_0(\tau)$, plotted against $\bar{r}\tau$. (c) Renormalized simulations of $P_0(\tau)$, plotted on a logarithmic axis against $\bar{r}\tau$.

Figure 6(c) contains the same data as Fig. 6(b), but with a logarithmic scale on the y axis. This gives a clear representation of the tail of the PDF. When $a = 0$, the tail is a straight line corresponding to exponential decay. For higher values of a there is a shoulder in the tail at around twice the mean. We consider the possibility that this shoulder is an artefact of simulation whereby two crossings appear within one time step so that a longer interval is falsely recorded. This is done by comparing the PDF simulated with the resolution used throughout this paper, and at twice that resolution. In Fig. 7 it can be seen that the shoulders are almost identical in
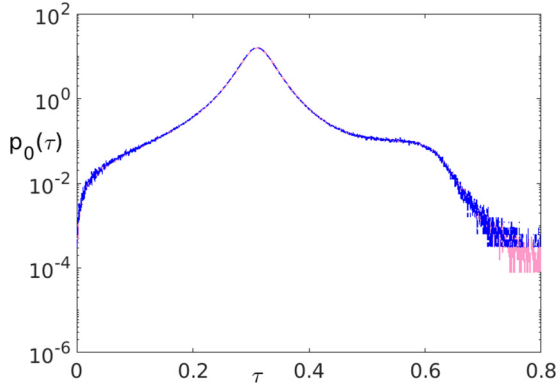
FIG. 7. Simulations of the PDF for $a = 10$ with the resolution used throughout this paper (dashed dark blue), and at twice this resolution (solid light pink).

both cases. The simulations of the smooth process $X(t)$ are of high enough resolution that misrecording zero crossings, that are distinct at the order of magnification of one time step, has no perceptible impact on the resulting density function. The explanation is then that occasionally the process turns when it is very close to zero, resulting in a zero-crossing interval of approximately twice the mean length. It is important to note that this "touch" of the zero line occurs very infrequently and is only perceptible on the logarithmic scale plots.

C. Correlations between the intervals

The correlation coefficient describes the correlation between the ith and $(i + j)$th intervals, τ_i and τ_{i+j}, and is defined as

$$\kappa_j = \frac{\langle \tau_i \tau_{i+j} \rangle - \langle \tau \rangle^2}{\sigma^2} \quad j > 0. \tag{7}$$

When intervals are independent of each other, they are uncorrelated and $\kappa_j = 0$. When $\kappa_j > 0$, intervals are positively correlated with $\kappa_j = 1$ corresponding to full correlation where the ith and $(i + j)$th intervals are the same length. When $\kappa_j < 0$, intervals are negatively correlated so that if the ith interval is long the $(i + j)$th interval is likely to be short.

Figure 8 shows the simulated results for the correlation coefficients κ_1 to κ_4. The graph of κ_1 is negative for small a, showing that successive interval lengths are anticorrelated in
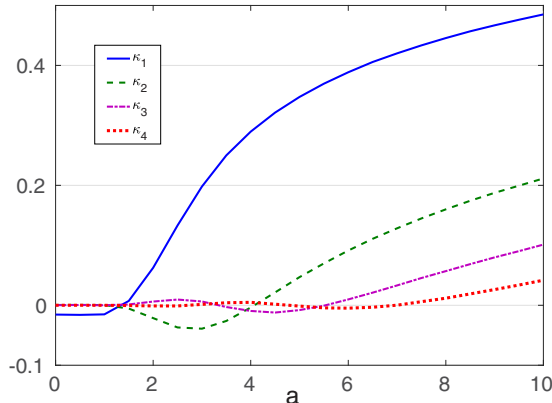

FIG. 8. Simulated values of the correlation coefficients (7).

this region. This indicates that zeros of the random process are repelled from each other where they are principally affected by the exponential factor in $\rho(\tau)$, $g(\tau) = \exp(-\tau^2/2)$. This is because the process is smooth and, unlike a fractal or subfractal process, cannot change sign or slope in an arbitrary short time. The intervals become positively correlated once the oscillations in $\rho(\tau)$ begin to occur within the characteristic width of the exponential function (i.e., for $\ell_1 < \ell_2$). This demonstrates that the process is becoming more regular, in accord with the behavior found for $F(T)$ in Sec. II C.

The higher-order correlation coefficients κ_2, κ_3, and κ_4 all start very close to zero. With progressively increasing a they then oscillate close to zero, through periods of correlation and anticorrelation, before becoming positive and strictly increasing. The number of oscillations observed corresponds to the order of the correlation coefficient, i.e., κ_2 crosses the axis twice and κ_4 crosses four times. This structure comes about through the interplay of the time scales of the cosine ℓ_1 and of the power law ℓ_2, described in Sec. III A. In the limit $\ell_1 \to 0$ all the $\kappa_i \to 1$, indicating a trend towards exact periodicity and determinism. These simulation results demonstrate that intervals between zero crossings are not independent of each other.

IV. CALCULATING THE INTERVAL VARIANCE

In this section we present McFadden's derivation of two expressions for the variance under the assumption that successive intervals are independent. The simulation results presented in the previous section demonstrate that the independent intervals assumption is not correct. We extend the work of McFadden to consider two possible assumptions for the structure of interval correlation. Again, we obtain expressions for the variance. In all three cases, the derivation of the expressions for the variance begins with some exact results: two infinite sums. The different assumptions about correlations are then substituted in and result in polynomials in the Laplace transform of $P_n(t)$. The second moment in the expansion of this Laplace transform is then identified so that expressions for the variance can be determined and numerically evaluated.

A. Exact results

Recall from Sec. III B that $P_n(\tau)$ is the density of the interval length between $n + 1$ successive events. Two infinite series of $P_n(\tau)$ were derived by McFadden [21].

The first relates to the clipped process of $X(t)$, which identifies the locations of the zero crossings, and is defined as

$$\xi(t) = \begin{cases} 1 & X(t) \geqslant 0 \\ -1 & X(t) < 0 \end{cases}.$$

The autocorrelation function of $\xi(t)$ is

$$R(\tau') = \langle \xi(t)\xi(t + \tau') \rangle,$$

from which it can be shown that

$$\frac{R''(\tau)}{4\bar{r}} = \sum_{n=0}^{\infty} (-1)^n P_n(\tau) \tag{8}$$

where $\bar{r}$ is the crossing rate (5).

McFadden derived a second infinite series relating $P_n(\tau)$ to $U(\tau)$ where $U(\tau)d\tau$ is defined to be the conditional probability that a zero occurs in the interval $(t + \tau, t + \tau + d\tau)$, given one occurs at t. If there is a zero in the interval $(t + \tau, t + \tau + d\tau)$, it must be either the first, second, third,...up to infinity and hence

$$U(\tau) = \sum_{n=0}^{\infty} P_n(\tau). \tag{9}$$

Deriving equations for the variance of the zero-crossing intervals requires the following Laplace transform:

$$u(s) = \mathcal{L}[U(\tau)], \tag{10}$$

$$r(s) = \mathcal{L}\left(\frac{R''(\tau)}{4\bar{r}}\right), \tag{11}$$

$$p_n(s) = \mathcal{L}[P_n(\tau)] \tag{12}$$

so that the infinite sums can be expressed as

$$r(s) = \sum_{n=0}^{\infty} (-1)^n p_n(s), \tag{13}$$

$$u(s) = \sum_{n=0}^{\infty} p_n(s). \tag{14}$$

Both these infinite sums, expressed in $P_n(\tau)$ or $p_n(s)$, are *exact results* for a general, symmetric, stationary, ergodic process, meaning any sample from the process must represent the average statistical properties of the entire process.

B. Assumption: Independent intervals

Making the *assumption* that successive intervals between zero crossings are statistically independent the the interval sums are given by convolutions of $P_0(t)$, or in terms of the Laplace transforms

$$p_n(s) = p_0(s)^{n+1}. \tag{15}$$

Substituting this into the infinite sums (13) and (14) obtains two independent equations for $p_0(s)$:

$$p_0(s) = \frac{r(s)}{1 - r(s)}, \tag{16}$$

$$p_0(s) = \frac{u(s)}{1 + u(s)}. \tag{17}$$

From the definition of the Laplace transform we obtain the moments of $P_0(\tau)$ from derivatives of $p_0(s)$ at $s = 0$. By matching coefficients of equal powers of s in the expansion of (16), expressions for $\langle \tau \rangle$ and $\langle \tau^2 \rangle$ are obtained. The resulting expression for the variance is then

$$\sigma_I^2 = \frac{2I}{\bar{r}}$$

with I defined as the integral

$$I = \int_0^{\infty} R(\tau)d\tau.$$

The function $u(s)$ cannot be expanded about the origin but the transform $v(s) = u(s) - \bar{r}/s$ enables expansions of $p_0(s)$

and $v(s)$ to be substituted into (17). We then obtain a second expression for the variance through matching powers of s:

$$\sigma_J^2 = \frac{1 + 2J}{\bar{r}^2}$$

where

$$J = \int_0^{\infty} [U(\tau) - \bar{r}]d\tau.$$

The evaluation of the integrals I and J depend on the precise distribution of the process. These two expressions for the variance, σ_I and σ_J, could be expected to match if, and only if, the assumption of statistical independence of intervals were correct.

Numerical evaluation

Evaluating the clipped autocorrelation function requires an integral of the bivariate density function for the process $X(t)$. The result for a Gaussian process is given by the van Vleck theorem [38]:

$$R(\tau) = \frac{2}{\pi} \arcsin[\rho(\tau)]. \tag{18}$$

For a Gaussian process, the function $U(\tau)$ has been determined by Rice [31] (Sec. 3.4) to be

$$U(\tau) = \frac{1}{\bar{r}\pi^2\left[1 - \rho^2(\tau)\right]^{3/2}}$$
$$\times \left[|A^2 - B^2|^{1/2} + B \arctan\left(\frac{B}{|A^2 - B^2|^{1/2}}\right)\right]$$

with A and B given in (6). These permit σ_I^2 and σ_J^2 to be evaluated by quadrature.

In Fig. 9 numerical evaluations of the variance in both cases are compared to results from simulations. Both σ_I^2 and σ_J^2 display the same overall behavior as the simulated variance with slight over- or underestimation of a similar
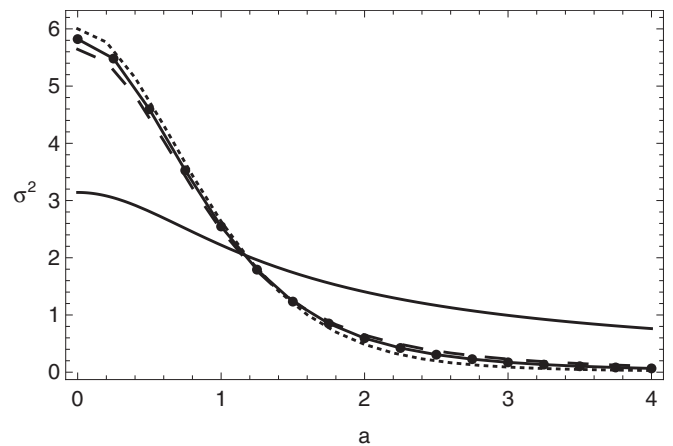
FIG. 9. The variance from simulations (circles) and numerical evaluation of the model σ_I^2 from (IV B) (dotted) and σ_J^2 from (IV B) (dashed) as well as the mean interval length via (5) (solid).

magnitude. The findings of the previous sections are affirmed, with the decreasing variance reflecting increasingly regular zero crossings.

The difference between the two results for the variance, although small, implies that intervals between zero crossings are not independent of each other. At $a \sim 1.3$, $\sigma_I^2 = \sigma_J^2$, suggesting that the intervals may be uncorrelated at this point, however simulation results show this is not the case and that this point does *not* correspond to $\kappa_j = 0$. We conclude that incorporating interval correlation is necessary.

C. Assumption: Interval correlation

A strategy for relaxing the assumption of statistical independence was suggested by McFadden [21] through the introduction of the undetermined function $a_n(s)$ into the assumed model so that

$$p_n(s) = a_n(s) p_0^{n+1}(s). \tag{19}$$

This relation is a generalization of (15), which followed when successive intervals were assumed to be independent of each other. The function $a_n(s)$ embodies information about correlation. As with the uncorrelated case, this relation will be substituted into the two infinite sums (13) and (14), and the second moment in the expansion of $p_0(s)$ will be identified so that two expressions for the variance can be found. Unlike the uncorrelated case, the extra degree of freedom introduced by $a_n(s)$ will enable these two expressions for the variance to be equated to each other. First, $a_n(s)$ must be determined.

It is possible to determine $a_n(s)$ using the fact that $p_n(s)$ is a moment generating function with expansion near the origin:

$$p_n(s) = 1 - \langle T \rangle s + \langle T^2 \rangle s^2 + O(s^4)$$

where

$$T = \sum_{j=1}^{n+1} \tau_j.$$

Noting that $\langle T \rangle = (n+1)\langle \tau \rangle$ the expansion for $a_n(s)$ follows:

$$a_n(s) = \frac{p_n(s)}{p_0(s)^{n+1}}$$

$$= 1 + \frac{s^2}{2}[\langle T^2 \rangle - (n+1)(n\langle \tau \rangle^2 + \langle \tau^2 \rangle)] + O(s^4).$$

The quantity $\langle T^2 \rangle$ contains terms of the form $\langle \tau_i \tau_j \rangle$ and so, in order to evaluate these terms, the correlation coefficient (7) is required. Then

$$\langle T^2 \rangle = \left\langle \left(\sum_{i=1}^{n+1} \tau_i \right)^2 \right\rangle = \left\langle \sum_{i=1}^{n+1} \tau_i \sum_{j=1}^{n+1} \tau_j \right\rangle$$

$$= 2 \sum_{j=1}^{n} (n-j+1)\langle \tau_i \tau_{i+j} \rangle + (n+1)\langle \tau^2 \rangle$$

$$= 2\sigma^2 \sum_{j=1}^{n} (n-j+1)\kappa_j + n(n+1)\langle \tau \rangle^2 + (n+1)\langle \tau^2 \rangle.$$

Combining these results yields the simpler form

$$a_n(s) = 1 + s^2 \sigma^2 \sum_{j=1}^{n} (n-j+1)\kappa_j \quad n > 0, \tag{20}$$

$$a_0(s) = 1. \tag{21}$$

Obtaining a closed form expression (involving only $\kappa = \kappa_1$) for $a_n(s)$ requires a suitable closure model for the κ_j's. In this paper we explore two models: a Markov chain model and a truncated model.

1. Markov chain correlation model

McFadden made the *assumption* that the intervals form a Markov chain yielding the closure condition $\kappa_j = \kappa^j$, where $\kappa = \kappa_1$, the correlation coefficient for consecutive intervals. Our simulation results in Fig. 8 suggest this is an appropriate model for large enough a.

Substituting the Markov chain closure condition into (20) yields

$$a_n(s) = 1 + \frac{s^2 \sigma^2 \kappa}{(1-\kappa)^2}[n - (n+1)\kappa + \kappa^{n+1}] + O(s^3). \tag{22}$$

This enables the evaluation of (19) in the infinite sums (13) and (14). In the uncorrelated, independent intervals case this resulted in two quadratic equations (16) and (17); the additional information about interval correlation contained in (22) results in the following cubic equations in $p_0(s)$:

$$r(s) = \frac{p_0}{1+p_0} - \frac{\kappa(\sigma s p_0)^2}{(1+p_0)^2(1+\kappa p_0)}, \tag{23}$$

$$u(s) = \frac{p_0}{1-p_0} + \frac{\kappa(\sigma s p_0)^2}{(1-p_0)^2(1-\kappa p_0)}, \tag{24}$$

which reduce to the uncorrelated case (16) and (17) when $\kappa = 0$.

By matching coefficients of equal powers up to $O(s^2)$ in (13) and (23) we obtain

$$\sigma_I^2 = \beta \left(\frac{1+\kappa}{1-\kappa} \right)$$

with

$$\beta = \frac{2I}{\bar{r}}.$$

Through doing so in (14) and (24), via the transform $v(s) = u(s) - \bar{r}/s$, we obtain a second expression for the variance:

$$\sigma_J^2 = \frac{\beta}{\alpha^2} \left(\frac{1-\kappa}{1+\kappa} \right)$$

with

$$\alpha = \left(\frac{2\bar{r}I}{1+2J} \right)^{\frac{1}{2}}.$$

The condition that $\sigma_I = \sigma_J > 0$ determines

$$\kappa = \frac{1-\alpha}{1+\alpha} \quad \text{and} \quad \sigma^2 = \frac{\beta}{\alpha}. \tag{25}$$

Figure 10 shows numerical evaluation of the variance and correlation coefficient in (25) plotted against results from
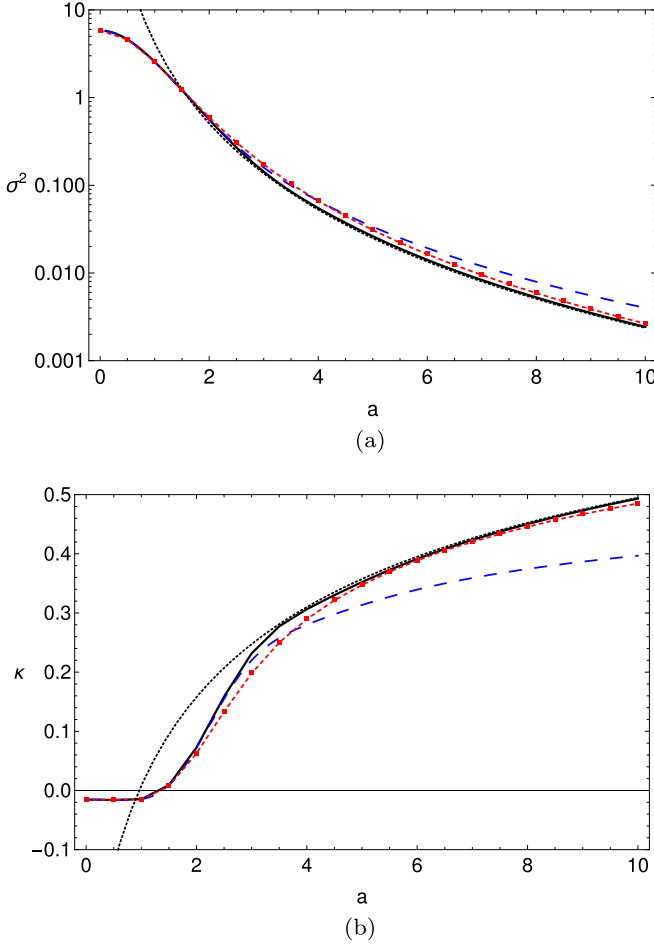
(a)

(b)

FIG. 10. The variance and first-order correlation coefficient of the interval between crossings as a function of a from simulations (red dashed with squares), from numerical analysis of the Markov chain model (25) (solid black) and its asymptotic limit (26) (dotted black), and from numerical analysis of the truncated model (31) (blue dashed). (a) The variance of the interval between crossings. (b) The interval correlation coefficient.

simulations. In the case of the variance, the model gives an accurate result, verifying that the theory is effective up to $O(s^2)$ and computation of the integrals in (25) is correct. The result for κ is good for small a; it then deviates slightly from the simulated results for $2 < a < 5$. This is the region where simulation results in Fig. 8 show that κ_2 and κ_3 are negative, whereas the Markov chain assumption has them as a power of κ_1, which is positive in this region. For larger a the model appears to reflect simulated results in Fig. 8 again, as only higher index κ_j's would be negative and their effect is smaller given that all the lower index κ_j's do appear to fit the model.

2. Asymptotic behavior of the variance and correlation coefficient under the Markov chain model

For large enough a, both the variance and the correlation coefficient (25) are described by a power law. This follows from numerical results which show that

$$\beta \sim \frac{8}{a^4} \quad \text{and} \quad \alpha \sim \left(\frac{8}{7a}\right)^{1/2}$$

as $a \to \infty$. Hence

$$\sigma^2 = \frac{\beta}{\alpha} \sim \left(\frac{56}{a^7}\right)^{1/2} \tag{26}$$

and

$$\kappa = \frac{1-\alpha}{1+\alpha} \sim \frac{1 - \left(\frac{8}{7a}\right)^{1/2}}{1 + \left(\frac{8}{7a}\right)^{1/2}} \tag{27}$$

as $a \to \infty$. Plots of these asymptotic results for σ^2 and κ are shown in Fig. 10.

The power-law decay of the interval variance and correlation demonstrates that the dynamics at play in this system are far from simple. On first glance, the variance in Fig. 10 might appear to decay exponentially or, like the autocorrelation function, according to a Gaussian function $\exp(-a^2)$. This is not the case, and the effect of the cosine term in the autocorrelation function is bound up in the intricacies resulting from nonstandard oscillatory integrals.

3. Truncated correlation model

The simulation results in Fig. 8 show that, while the correlation coefficients do appear to form a Markov chain for large a, this is not an appropriate assumption for an intermediate regime in a. Therefore we propose the equally tractable *assumption* that only successive intervals are correlated. That is, $\kappa_j = 0$ for $j \geqslant 2$, which gives

$$a_n(s) = 1 + n\sigma^2 s^2 \kappa + O(s^3), \tag{28}$$

whereupon inserting this and (19) into the infinite sums (13) and (14) yields quadratic equations for $p_0(s)$:

$$r(s) = \frac{p_0}{1 + p_0} - \frac{\kappa(\sigma s p_0)^2}{(1 + p_0)^2}, \tag{29}$$

$$u(s) = \frac{p_0}{1 - p_0} + \frac{\kappa(\sigma s p_0)^2}{(1 - p_0)^2}, \tag{30}$$

which reduce to the uncorrelated result (16) and (17) when $\kappa = 0$.

Following the same methods as before,

$$\sigma^2 = \frac{1}{2}\left(\beta + \frac{\beta}{\alpha^2}\right) \quad \text{and} \quad \kappa = \frac{1}{2}\left(\frac{1-\alpha^2}{1+\alpha^2}\right). \tag{31}$$

The variance and correlation coefficient under this model are shown in Fig. 10. The truncated model predicts the variance accurately, although not as well as the Markov chain model for larger a.

4. Discussion of correlation assumptions

Comparing results for the correlation coefficient κ in Fig. 10(b), the Markov chain proves to be a far better assumption for larger a. In fact, under the truncated model, the maximum value κ can take is $1/2$ as opposed to the Markov chain model where it approaches 1 in agreement with simulations. This illustrates that as $a \to \infty$ the higher-order correlations $\kappa_2, \kappa_3 \ldots$ become more important. The truncated model does, however, provide a slight improvement on the Markov chain assumption in the intermediate region $2 < a < 4$, where the Markov chain model has $\kappa_2 > 0$ when in fact

simulation results in Fig. 8 show that $\kappa_2 < 0$. As $a \to 0$, the truncated model is qualitatively and quantitatively correct, getting the magnitude of the anticorrelation in this region correct.

V. CALCULATING THE DENSITY FUNCTION

Following the work of McFadden [20,21], incorporating correlation is achieved through the assumption that the interval densities are linked multiplicatively in the frequency domain with some unknown function of the frequency variable $a_n(s)$. In the previous section, that function is found up to $O(s^2)$ by matching coefficients in the expansions of interval densities. This methodology led to accurate predictions of the interval length variance, in the regions where the interval correlation closure condition was appropriate. The success of this method demonstrates that the theory is correct up to $O(s^2)$. In this section, by considering poles in the Laplace transform of the density function, we predict the tail of the density function for small a, where $|s| < 1$, and propose further work towards a global expression for the tail of the density function.

A. Persistence

Persistence is the probability $P_e(\tau)$ that there is no zero crossing by a Gaussian process in the interval $[0, \tau]$. Persistence is related to the PDF $P_0(\tau)$ for the intervals τ between successive crossings by

$$P_e(\tau) = \int_\tau^\infty P_0(t)dt.$$

Results by Olla [39] and Eichner *et al.* [40] state that, for sufficiently large τ, the form of the tail of $P_0(\tau)$ depends on the autocorrelation function. Specifically, if $\rho(\tau) \sim |\tau|^{-\gamma}$ with $\gamma > 1$, or if it is exponentially bounded such that $\rho(\tau) \sim \exp(-|\tau|^\gamma)$, as is the case for the autocorrelation function considered in this paper, then the asymptotic form of $P_0(\tau)$ does not depend on γ and is given by $P_0(\tau) \sim \exp(-\theta\tau)$. As it also describes the exponential tail of the persistence $P_e(\tau)$, θ is referred to as the persistence parameter. It relates to the length of time until the process changes state and describes how steep the tail of the interevent PDF is. Previous sections have shown that, as the autocorrelation function becomes more oscillatory, the variance of the interevent intervals decreases. Equivalently, the PDF will have a steeper tail, and the persistence parameter will increase.

The persistence parameter is examined through the structure of $p_0(s) = \mathcal{L}P_0(\tau)$. The tail of the interevent density function is $P_0(\tau) \sim \exp(-\theta\tau)$ and the Laplace transform of such an exponential function is

$$\mathcal{L}[\exp(-\theta\tau)] = \frac{1}{s + \theta}.$$

Hence we expect the Laplace transform of $P_0(\tau)$ to have a simple pole at $s = -\theta$. Consequently the location of the pole in $p_0(s)$ determines the persistence parameter.
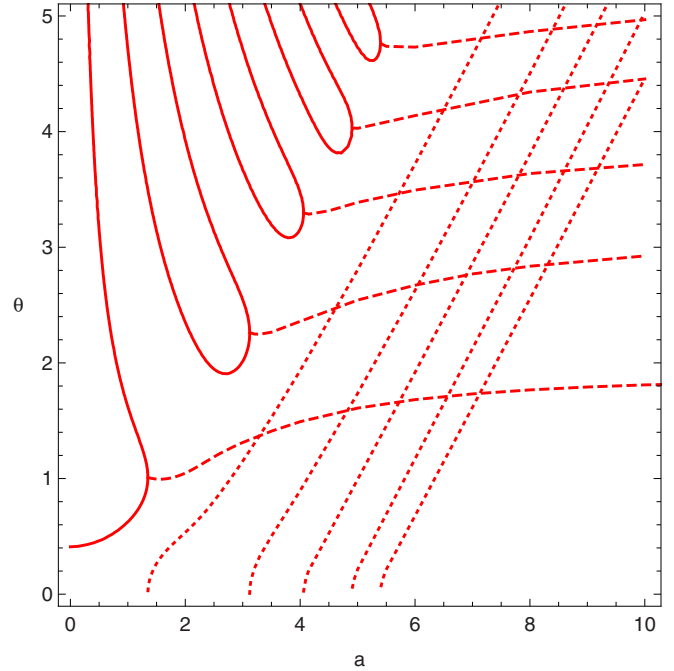

FIG. 11. Location of the poles in the Laplace transform of the interevent density function under the uncorrelated assumption given by (32). Real poles are solid lines; complex poles are made up of a real part (dashed) and imaginary part (dotted).

B. Uncorrelated intervals

In the uncorrelated model, $p_n(s) = p_0(s)^{n+1}$, the equation for $p_0(s)$ in terms of $r(s)$ (16) is

$$p_0(s) = \frac{r(s)}{1 - r(s)},$$

which indicates that $p_0(s)$ has a pole at the (negative) value of $s = -\theta$ that solves

$$r(-\theta) - 1 = 0. \tag{32}$$

The asymptotic form of the interevent distribution will then be $P_0(\tau) \sim \exp(-\theta\tau)$ where the persistence parameter θ describes the rate of decay.

Due to the oscillatory nature of $\rho'(\tau)$, there are in fact multiple poles of $p_0(s)$. These occur at negative values of $s = -z_j$, where $z_1 < z_2 < z_3 \ldots$ are the solutions to

$$\frac{-z}{\pi \bar{r}} \int_0^\infty \frac{\rho'(\tau) \exp(z\tau)}{[1 - \rho(\tau)^2]^{1/2}} d\tau - 1 = 0$$

resulting from inserting (11) and (18) into (32).

The topology of the location of the poles in $p_0(s)$ is shown in Fig. 11. The real-value locations are established by performing a numerical contour plot of (V B) with a single contour at zero, where the integral is evaluated numerically. Because the complex roots arise from the point at which two real roots coalesce, it is possible to track them from this point.

For a given value of a, taking a vertical slice in Fig. 11 gives the multiple roots of (32). For $a < 1.3$ there are infinitely many real-valued roots, the first of which are observed in the plot. At $a \approx 1.35$ the smallest two real roots coalesce, resulting in a complex root, the real and imaginary parts of which are plotted
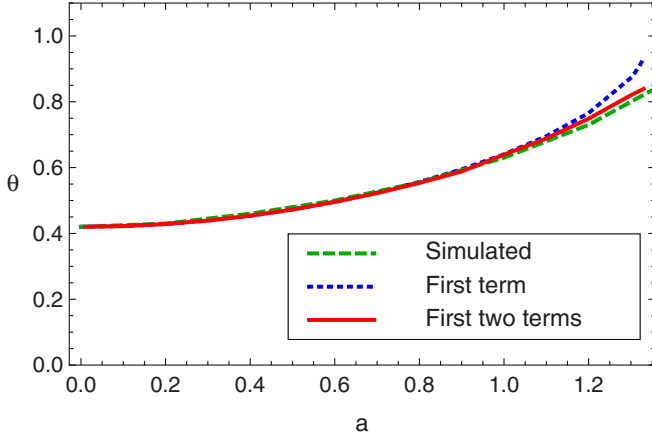
FIG. 12. The persistence parameter θ, from simulations (green dashed), from considering only the first term in (33) (blue) and from considering the first two terms in (33) (red).
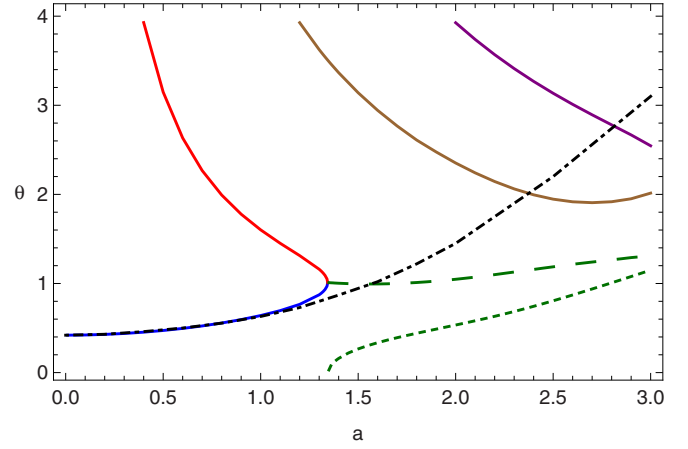

FIG. 13. The real (solid colored) and complex (real part, dashed green; imaginary part, dotted green) poles of (32), as well as the simulated value of θ (dot-dashed black).

by dashed and dotted lines, respectively. More complex roots emerge as further real-valued roots coalesce.

For a given value of a, there exists some $m > 0$ for which the subsequent poles, $z_{m+1}, z_{m+2} \ldots$ are purely real and positive. Furthermore, numerical results show that as $n \to \infty$ the interval between these poles $z_{n+1} - z_n$ approaches π/a so that $z_{n+k} = z_n + k\pi/a$.

Such a spectrum of infinitely many poles in $p_0(s)$ has not been observed before in the context of the zero-crossing problem.

Calculating the persistence parameter for small a

The locations of the first few poles such that $s = -z_j$, where $z_1 < z_2 < z_3 \ldots$, are shown in Fig. 13, alongside the simulated value of the persistence parameter θ.

In order to estimate θ, the function $p_0(s)$ can be approximated close to each pole. Expanding $r(s)$ about the location of a pole $s = -z_j$,

$$r(s) = r(-z_j) + r'(-z_j)(s + z_j)$$
$$+ \frac{r''(-z_j)}{2}(s + z_j)^2 + O[(s + z_j)^3]$$

with $r(-z_j) = 1$, which upon insertion into (32) gives

$$p_0(s) \approx \frac{-1}{[r'(z_j)](s + z_j)}.$$

Hence the tail of the distribution $P_0(\tau)$ is given by the sum of the relative contribution from each of the poles:

$$\lim_{\tau \to \infty} P_0(\tau) \sim \mathcal{L}^{-1}\left(\sum_j \frac{-1}{r'(z_j)(s + z_j)}\right)$$

and the persistence parameter can be determined from a linear fit to

$$\theta = -\frac{d}{d\tau} \ln \left| \mathcal{L}^{-1}\left(\sum_j \frac{-1}{r'(z_j)(s + z_j)}\right) \right|. \tag{33}$$

Figure 12 compares θ obtained from simulations, with that obtained from calculations including only the first term

in (33) as well as including the first two terms. For small a including only the first term is sufficient. The magnitude of the least negative pole z_1 coincides with the value of θ obtained from (33). As the location of the second real pole nears the first, its contribution in (33) becomes significant [note that $r'(-z_1)$ and $r'(-z_2)$ are necessarily of opposite sign] creating logarithmic modifications to the tail of the PDF which persist even for $\tau/\langle\tau\rangle > 1$. The effect of these adjustments is that, when including the second term in calculations, the persistence parameter is *reduced* from that value predicted by the first regarded in isolation, giving an improved estimate.

The first two real roots merge at $a \approx 1.34$, whereupon the root becomes complex, the real part being shown in Fig. 13 by the dashed curve and the imaginary part being shown by the dotted curve. When determining θ under (33), the value of $\mathrm{Re}(z_1)$ places an upper bound on the value calculated for θ. Figure 13 shows that for $a > 1.6$ the simulated value of θ exceeds $\mathrm{Re}(z_1)$ and is increasing at a far greater rate. The simulated values for θ are much higher, and hence the decay of the tail is much faster, than this model will predict. In this region, the correlations between intervals must be incorporated into the model.

C. Correlated intervals

In Sec. IV C the variance and correlation coefficients were effectively modeled through the introduction of the function $a_n(s)$ into the assumed model so that

$$p_n(s) = a_n(s) p_0^{n+1}(s).$$

Using the fact that $p_n(s)$ is a moment generating function, $a_n(s)$ was determined up to $O(s^2)$ under a suitable closure condition for the correlation coefficients. Considering $a < 3$ then, the truncated correlation model is appropriate, for which solving the quadratic (29) in favor of $p_0(s)$ gives

$$p_0(s) = \frac{[2r(s) - 1] \pm [1 - 4\kappa\sigma^2 s^2 r(s)]^{1/2}}{-2[r(s) - 1 + \kappa\sigma^2 s^2]}.$$

Taking the "+" solution, poles of $p_0(s)$ occur where the denominator vanishes when $s \to -\theta$, which now becomes

the solution of

$$r(-\theta) - 1 = -\kappa \sigma^2 \theta^2. \tag{34}$$

Note that this is not a linear perturbation of the uncorrelated assumption result in (32) (the correlation coefficient features explicitly and is coupled with σ^2 but retrieves it if $\kappa = 0$).

Figure 14 shows the topology of the poles for the correlated case, and in comparison to the uncorrelated case. The correlated case displays very similar results to the uncorrelated case, but the way in which the real-valued poles coalesce is slightly different. As $\sigma^2 \sim (56/a^7)^{1/2}$ for $a \gg 1$ (26) and $|\kappa| \leqslant 1$ the roots of the correlated case (34) approach those of the uncorrelated case (32). This can be seen in Fig. 14(b); although the structure is different when they first emerge, with increasing a the complex roots tend to the same value as found in the uncorrelated case.

Again, the function $p_0(s)$ can be approximated close to each pole. Expanding $r(s)$ about the location of a pole $s = -z_j$,

$$r(s) = r(-z_j) + r'(-z_j)(s + z_j)$$
$$+ \frac{r''(-z_j)}{2}(s + z_j)^2 + O[(s + z_j)^3]$$

with $r(-z_j) = 1 + \kappa \sigma^2 s^2$, which upon insertion into (V C) gives

$$p_0(s) \approx \frac{2\kappa \sigma^2 z_j^2 - 1}{[r'(z_j) + 2\kappa \sigma^2 z_j](s + z_j)}.$$

The persistence parameter can then be determined from a linear fit to

$$\theta = -\frac{d}{d\tau} \ln \left| \mathcal{L}^{-1} \left(\sum_j \frac{2\kappa \sigma^2 z_j^2 - 1}{f'(z_j)(s + z_j)} \right) \right|$$

with $f(s) = r(s) - \kappa \sigma^2 s^2$.

Estimating θ in this way does not improve on the uncorrelated result because $\kappa \sigma^2 \ll 1$. Again, $\mathrm{Re}(z_1)$ places an upper bound on the value calculated for θ. It is clear from Fig. 14 that the truncated correlated model does not significantly improve upon the uncorrelated one. There is also no significant improvement under the Markov chain assumption. In both cases, the problem lies in the expansion of $a_n(s)$.

Using polynomial expansions to locate poles in $p_0(s)$ is only appropriate in the region where the s expansion for $a_0(s)$ applies. Under both closure conditions $a_0(s)$ is approximated as

$$a_n(s) = 1 + s^2 \sigma^2 \kappa f(n, \kappa) + o(s^2)$$

for some function f such that $f(0, \kappa) = 0$ and $f(n, \kappa)$ is positive when $n \geqslant 0$ and $0 < \kappa < 1$. As $a \to \infty$, $\sigma^2 \kappa \to 0$, which means that the $O(s^2)$ expansion of $a_n(s) \to 1$ and hence the correlated intervals model approaches the uncorrelated intervals model under both closure conditions. Simulation results show that, as $a \to \infty$, κ has far greater influence than this model would suggest. The PDF becomes more singular so that $P_n(\tau)$ tends towards a delta function located at the mean interval spacing $(n + 1)\langle \tau \rangle$.
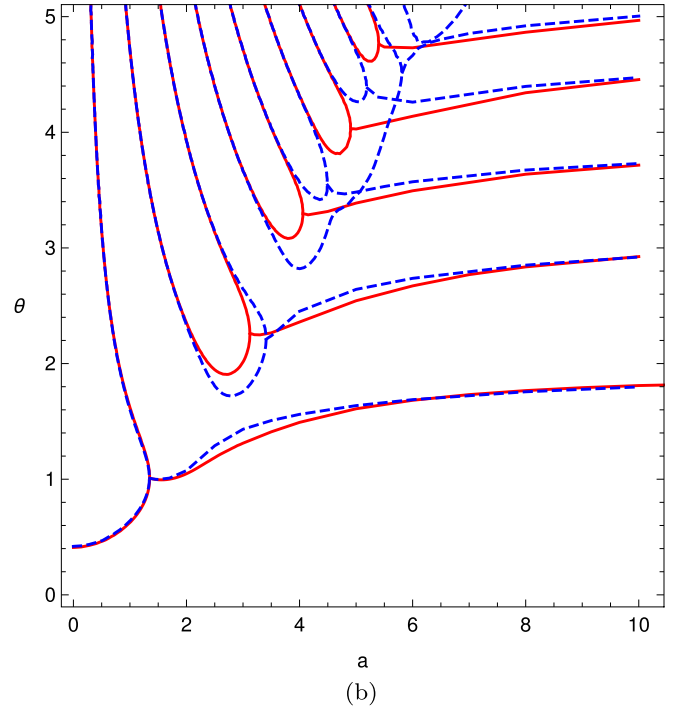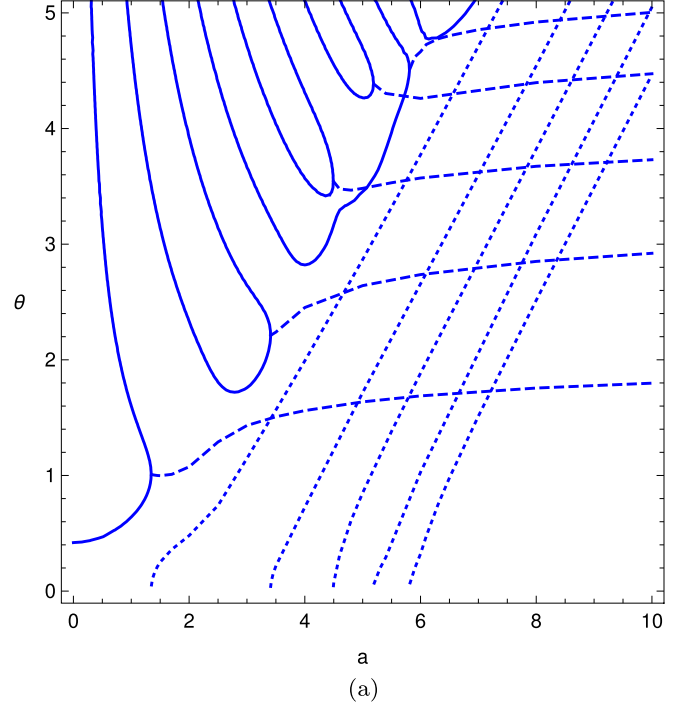

(a)

(b)

FIG. 14. The poles in the Laplace transform of the interval density function, in the correlated intervals case and in comparison to the uncorrelated. (a) The poles in the correlated intervals case given by (34). Real poles (solid) coalesce to form complex poles made up of a real part (dashed) and imaginary part (dotted). (b) The real part of poles in the correlated case (dashed blue) (34) and the uncorrelated case (solid red) (32).

D. Transitional model

The above model for $p_n(s)$ could never describe a delta function and so, in the situation when $a \to \infty$, an adapted
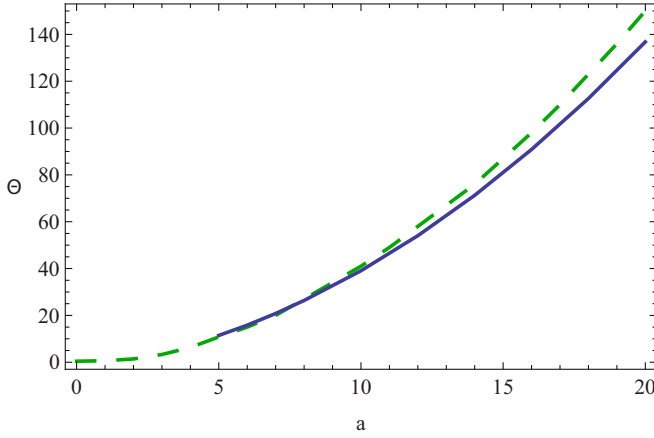
FIG. 15. The persistence parameter with $\mu = 4.5$ from simulations (dashed green) and estimated for $a \geqslant 5$ via (36) and (37) (solid blue).

model is designed to account for this:

$$p_n(s) = \hat{p}_0[(1 - \kappa)^\mu s]^{n+1} \exp\left[-(n+1)\kappa \langle \tau \rangle s\right]$$

for some $\mu > 0$ and where $\hat{p}_0(s)$ satisfies the uncorrelated model which was shown to be sufficient for smaller a:

$$\hat{p}_n(s) = \hat{p}_0(s)^{n+1}. \tag{35}$$

When $\kappa = 0$ this model has the same structure as the uncorrelated model (35). As $a \to \infty$, $\kappa \to 1$ and

$$p_n(s) = \exp\left[-(n+1)\langle \tau \rangle s\right],$$

which is the Laplace transform of a delta function located at the mean interval spacing.

Essentially this model provides a transition from the PDF being a solution to the uncorrelated model (valid for small a) to the PDF being a delta function at the mean interval length (valid for infinitely large a). As $a \to \infty$, the PDF suggested by (35) is compressed and the influence of the delta function increases.

For large a the asymptotic result for κ (27) is

$$\kappa \sim \frac{1 - \alpha}{1 + \alpha} \sim \frac{1 - \left(\frac{8}{7a}\right)^{1/2}}{1 + \left(\frac{8}{7a}\right)^{1/2}},$$

which is a good approximation when $a \geqslant 5$. In this region the poles of $p_0(s)$ then occur at the poles of $\hat{p}_0[(1 - \kappa)^\mu s]$ which are given by (32) as $s = -z_j$, the solution to

$$r[-(1 - \kappa)^\mu z_j] - 1 = 0. \tag{36}$$

The persistence parameter is then estimated as

$$\theta = \mathrm{Re}(z_1) \tag{37}$$

where z_1 is the smallest root.

Figure 15 shows the persistence parameter from simulations, and estimated via (36) and (37) with $\mu = 4.5$, for the region $a \geqslant 5$ where the asymptotic result for κ is accurate. The transitional model captures the rate of increase in the persistence parameter as the PDF tends towards a delta function for large a.

E. Future work

By considering poles in the Laplace transform of the density function, accurate predictions of the density function tail have been made for small a, where $|s| < 1$. However, it is not possible to locate poles in $p_0(s)$ where $|s| > 1$. Doing so would require the global form of $a_n(s)$.

One plausible model for tackling this problem would be to renormalize the function so that

$$a_n(s) = 1 \pm \kappa \sigma^2 s^2 \exp\left[-|f(s)|\right] \tag{38}$$

with $f(0) = 0$. This model incorporates terms of the form

$$\langle \tau_i \tau_{i+j} \tau_{i+j+k} \ldots \rangle. \tag{39}$$

The related higher-order correlations $\kappa_{i,j,k,\ldots}$ must all tend towards unity as determinism is approached when $a \to \infty$. In addition, further analysis of the persistence would be helped with more accurate simulations extending further into the tail of the distribution. Because intervals of these lengths are extremely rare, this would require a great deal more time and computational power.

VI. SUMMARY

The model presented in this paper explores systematically the changes that occur between a random signal and a deterministic one. Study of the effects of oscillation in the autocorrelation function has revealed a sliding scale of regularity in the zero crossings of Gaussian processes. For both the power-law autocorrelation function and the Gaussian limit case, more oscillations in the autocorrelation function mean zero crossings occur at more regular intervals. As zero crossings become more regular, the random intervals between them have reduced variance and a more localized, tending to singular, probability density function. This will prove useful for modeling any process upon which there is a periodic variation, for example the diurnal and annual variations implicit in weather, climate, traffic, energy demand, sleep patterns, etc., or in analysis of signals which result from some combination of periodicity and random noise such as in interferometry or tomography.

This paper demonstrates that the entire structure of the autocorrelation function of the random process is the principal cause for the rich phenomenology exhibited by the derived process of the interevent intervals. In particular, the oscillatory behavior in the autocorrelation function is a way of punctuating a random process by deterministic features. The way these become manifested is subtle, first involving an interplay between the characteristic scale sizes associated with the higher-order statistics, but eventually cascading throughout the entire process as it becomes progressively more correlated. Divining how these scale sizes emerge from the properties of the autocorrelation function remains an area for fruitful investigation.

[1] S. N. Majumdar, C. Sire, A. J. Bray, and S. J. Cornell, Nontrivial Exponent for Simple Diffusion, Phys. Rev. Lett. **77**, 2867 (1996).

[2] W. B. Davenport, Jr. and W. L. Root, *An Introduction to the Theory of Random Signals and Noise* (IEEE, New York, 1987).

[3] R. G. Bachu, S. Kopparthi, B. Adapa, and B. D. Barkana, Voiced/unvoiced decision for speech signals based on zero-crossing rate and energy, in *Advanced Techniques in Computing Sciences and Software Engineering* (Springer, New York, 2010), p. 279.

[4] P. E. William and M. W. Hoffman, Identification of bearing faults using time domain zero-crossings, Mech. Syst. Signal Process. **25**, 3078 (2011).

[5] R. Wiley, Approximate FM demodulation using zero crossings, IEEE Trans. Commun. **29**, 1061 (1981).

[6] G. Lindgren, Wave analysis by slepian models, Probab. Eng. Mech. **15**, 49 (2000).

[7] G. Lindgren, Horseshoe-like patterns in first-order 3d random gauss-lagrange waves with directional spreading, Waves Rand. Complex Media **25**, 729 (2015).

[8] J. D. Salas, C. Chung, and A. Cancelliere, Correlations and crossing rates of periodic-stochastic hydrologic processes, J. Hydrol. Eng. **10**, 278 (2005).

[9] P. J. Edwards and R. B. Hurst, Level-crossing statistics of the horizontal wind speed in the planetary surface boundary layer, Chaos: An Interdisc. J. Nonlinear Sci. **11**, 611 (2001).

[10] P. Douglas, The persistence exponent of DNA, Biophys. Chem. **110**, 59 (2004).

[11] M.-C. Wu, M.-C. Huang, H.-C. Yu, and T. C. Chiang, Phase distribution and phase correlation of financial time series, Phys. Rev. E **73**, 016118 (2006).

[12] M. Constantin and S. Das Sarma, Volatility, persistence, and survival in financial markets, Phys. Rev. E **72**, 051106 (2005).

[13] P. H. Brill, An embedded level crossing technique for dams and queues, J. Appl. Probab. **16**, 174 (1979).

[14] I. Rychlik, On some reliability applications of Rice's formula for the intensity of level crossings, Extremes **3**, 331 (2000).

[15] G. Lindgren, Wave-length and amplitude in Gaussian noise, Adv. Appl. Probab. **4**, 81 (1972).

[16] T. Malevich, Asymptotic normality of the number of crossings of level zero by a Gaussian process, Theory Probab. Appl. **14**, 287 (1969).

[17] I. Blake and W. Lindsey, Level-crossing problems for random processes, IEEE Trans. Inf. Theory **19**, 295 (1973).

[18] E. Wong, Some results concerning the zero-crossings of Gaussian noise, SIAM J Appl. Math. **14**, 1246 (1966).

[19] L. R. M. Wilson, K. I. Hopcraft, and E. Jakeman, The influence of oscillatory correlation on the zero crossings of gaussian processes, in *Vulnerability, Uncertainty, and Risk: Quantification, Mitigation, and Management*, edited by M. Beer, S.-K. Au, and J. W. Hall (American Society of Civil Engineers, Reston, Virginia, 2014), p. 1856.

[20] J. A. McFadden, The axis-crossing intervals of random functions, IRE Trans. Inform. Theory **2**, 146 (1956).

[21] J. A. McFadden, The axis-crossing intervals of random functions II, IRE Trans. Inform. Theory **4**, 14 (1958).

[22] D. M. Gordon, Control without hierarchy, Nature (London) **446**, 143 (2007).

[23] I. Rosenfield and E. Ziff, Evolving evolution, The New York Review of Books **53** (2006), http://www.nybooks.com/articles/2006/05/11/evolving-evolution/.

[24] J. Gerhart, M. Kirschner, and E. S. Moderbacher, *Cells, Embryos, and Evolution: Toward a Cellular and Developmental Understanding of Phenotypic Variation and Evolutionary Adaptability* (Blackwell Science Malden, Oxford, 1997).

[25] M. Mitchell, *Complexity: A Guided Tour* (Oxford University Press, Oxford, 2009).

[26] N. Wiener, Generalized harmonic analysis, Acta Math. **55**, 117 (1930).

[27] A. Khintchine, Korrelationstheorie der stationären stochastischen prozesse, Math. Ann. **109**, 604 (1934).

[28] E. Jakeman and K. D. Ridley, *Modeling Fluctuations in Scattered Waves*, 1st ed. (Taylor & Francis, London, 2006).

[29] R. Leadbetter, G. Lindgren, and H. Rootzén, *Extremes and Related Properties of Random Sequences and Processes*, Springer Series in Statistics (Springer-Verlag, Berlin, 1983).

[30] M. Abramowitz and I. A. Stegun, *Handbook of Mathematical Functions: With Formulas, Graphs, and Mathematical Tables*, Dover Books on Mathematics (Dover, New York, 2012).

[31] S. O. Rice, Mathematical analysis of random noise, in *Selected Papers on Noise and Stochastic Processes*, edited by N. Wax (Dover, New York, 1954).

[32] U. Fano, Ionization yield of radiations II: The fluctuations of the number of ions, Phys. Rev. **72**, 26 (1947).

[33] U. T. Eden and M. A. Kramer, Drawing inferences from Fano factor calculations, J. Neurosci. Meth. **190**, 149 (2010).

[34] C. W. J. Beenakker, M. Patra, and P. W. Brouwer, Photonic excess noise and wave localization, Phys. Rev. A **61**, 051801 (2000).

[35] H. Steinberg, P. M. Schultheiss, C. A. Wogrin, and F. Zweig, Short-time frequency measurement of narrow-band random signals by means of a zero counting process, J. Appl. Phys. **26**, 195 (1955).

[36] E. Jakeman and K. D. Ridley, Signal processing analog of phase screen scattering, J. Opt. Soc. Am. A **15**, 1149 (1998).

[37] I. G. Usoskin and K. Mursula, Long-term solar cycle evolution: Review of recent developments, Sol. Phys. **218**, 319 (2003).

[38] J. H. van Vleck and D. Middleton, The spectrum of clipped noise, Proc. IEEE **54**, 2 (1966).

[39] P. Olla, Return times for stochastic processes with power-law scaling, Phys. Rev. E **76**, 011122 (2007).

[40] J. F. Eichner, J. W. Kantelhardt, A. Bunde, and S. Havlin, Statistics of return intervals in long-term correlated records, Phys. Rev. E **75**, 011128 (2007).